

# Towards a digital twin realization of the blade system design study wind turbine blade

Alessandro Baldassarre<sup>1a</sup>, Alessandro Ceruti<sup>\*2</sup>, Daniel N. Valyou<sup>3b</sup> and Pier Marzocca<sup>4c</sup>

<sup>1</sup>Department of Mechanical and Aeronautical Engineering MAE, Clarkson University,  
8 Clarkson Avenue, Potsdam, NY 13699-5725, USA

<sup>2</sup>Department of Industrial Engineering DIN, University of Bologna, Viale del Risorgimento 2, 40136 Bologna, Italy

<sup>3</sup>School of Engineering, Clarkson University, 8 Clarkson Avenue, Potsdam, NY 13699-5725, USA

<sup>4</sup>School of Engineering, Aerospace Engineering and Aviation, RMIT University, Bundoora VIC 3083, Australia

(Received May 19, 2017, Revised December 13, 2018, Accepted December 17, 2018)

**Abstract.** This paper describes the application of a novel virtual prototyping methodology to wind turbine blade design. Numeric modelling data and experimental data about turbine blade geometry and structural/dynamical behaviour are combined to obtain an affordable digital twin model useful in reducing the undesirable uncertainties during the entire turbine lifecycle. Moreover, this model can be used to track and predict blade structural changes, due for example to structural damage, and to assess its remaining life. A new interactive and recursive process is proposed. It includes CAD geometry generation and finite element analyses, combined with experimental data gathered from the structural testing of a new generation wind turbine blade. The goal of the research is to show how the unique features of a complex wind turbine blade are considered in the virtual model updating process, fully exploiting the computational capabilities available to the designer in modern engineering. A composite Sandia National Laboratories Blade System Design Study (BSDS) turbine blade is used to exemplify the proposed process. Static, modal and fatigue experimental testing are conducted at Clarkson University Blade Test Facility. A digital model was created and updated to conform to all the information available from experimental testing. When an updated virtual digital model is available the performance of the blade during operation can be assessed with higher confidence.

**Keywords:** wind turbine; digital twin; finite element method; composite materials; modelling and simulation; design

## 1. Introduction

The percentage of the wind energy which can be captured by the turbine is strongly related to the efficiency of the blade aerodynamic design (Luhur *et al.* 2016), and a proper structural design is necessary to withstand loads due to centrifugal forces, aerodynamic lift, drag and moment on the blade, as well as generated and imposed vibrational loads, both with constant velocity and gusty winds. In this context the wind turbine blade is one of the most critical components of the whole wind turbine system. It is important to note that wind turbine blades can be subjected to highly unpredictable environmental dynamic loads during their operational life, which can lead to catastrophic failure. Large and frequent fluctuations in wind intensity and direction (Seshaiah and Sukkiramathi 2016) can cause severe stress/strain on wind turbine blades and, as suggested by Rezaee and Aly (2016), dynamics loads close to the resonance frequencies of the blade can amplify these damaging loads. Optimal blade design is necessary to increase the aerodynamic efficiency and structural strength (Ghasemi *et al.* 2014).

Simulation tools are necessary for effective design and structural verification in order to reduce time to market and development costs. In this framework, studies and analyses should be carried out to determine the best strategies for designing wind turbine blades to minimize blade failures with an optimal structural and aerodynamic design. At first glance producing CAD models and conducting FEM analysis for a wind turbine are not highly demanding tasks. However, each blade is unique due to blade to blade variation caused by many factors such as production tolerances, variance in materials from their nominal material properties, variability due to operational management practices, and environmental factors including humidity, temperature, and ultraviolet exposure during composite manufacturing, as well as the impact of aging on the blades. Typically, safety factors are employed during the design process to account for uncertainties in the design and manufacturing and as to mitigate these effects since there is no feedback between the digital model and the blade as it is produced.

When a CAD model and a finite element model of the product to be manufactured are developed, its structural properties are assumed from average material sheets, sizing is carried out and then the product is manufactured. There is no feedback between the blade's measured performance and the digital model. Modern engineering can exploit powerful computational capabilities in conjunction with sensor data and data analytics to generate far more robust and accurate structural models than the current one. A new paradigm

\*Corresponding author, Assistant Professor  
E-mail: [alessandro.ceruti@unibo.it](mailto:alessandro.ceruti@unibo.it)

<sup>a</sup> Ph.D. Student

<sup>b</sup> Ph.D. Student

<sup>c</sup> Professor, Associate Dean of Engineering

called the Digital Twin is emerging in this framework. The concept introduced in 2017 by Grieves and Vickers (2017) combines modern computational capabilities and sensor technologies to improve the fidelity of a virtual model to be used in the product lifecycle predictions. This means that the virtual model can describe more accurately the product performance during complex operations; it can also be used to support future products development and to predict failures or other anomalies during its operational life. Using the terminology by Grieves, the Digital Twin reduces undesirable uncertainties during the lifecycle of a product. The Digital Twin concept has been applied by Cerrone *et al.* (2014) to predict the direction of crack propagation in specimens where small manufacturing differences lead to completely different crushing modalities: also in this case, updating the digital model of the production part enhances the ability of the model to effectively predict structural performance. Improving the accuracy of wind turbine blade structural performance predictions can be particularly useful since turbines are often located in residential, commercial and community areas with potentially catastrophic consequences (Ashrafi *et al.* 2016) in case of failures. Moreover, the blade to blade variations of manufactured wind turbine blades are sufficiently high that a blade can present significant differences in structural response from nominal design values.

Small wind turbine blade safety is of particular concern because current standards (American Wind Energy Association safety standard, American National Standard Institute Essential Requirements, and the International Electro-technical Commission) do not require extensive physical testing, while static and fatigue structural testing is required for turbines with more than 200 m<sup>2</sup> swept area (roughly corresponding to a blade 8 meter long).

This paper will focus the attention on the development of a Digital Twin model of a heavily researched wind turbine blade, the Sandia National Labs BSDS (Blade System Design Study) described by Berry (2008). This blade has been designed from a number of airfoils of varying chord length, with a material layup made primarily of fibreglass composite, balsa wood and epoxy matrix, with a carbon fibre spar cap reinforcement. The thin shell is reinforced with an internal central spar web and pre-twist is applied along the blade's span. Details on the BSDS features can be found in several references, including Paquette and Veers (2007). The New York State Energy Research and Development Authority (NYSERDA) funded blade test facility operated by Clarkson University is used in this research. The blade test facility capabilities are described in Valyou *et al.* (2015).

The blade static and dynamic properties have been investigated in several papers. Tartibu *et al.* (2012) describe a numerical procedure to determine the blade natural frequencies and compare them with experimental tests. Griffith (2010) introduces a methodology to validate the blade structural dynamic properties, including techniques for experimental quantification of uncertainty in the modal parameters. Specific to large structures, FEM analysis and optimization of a 70 meter long wind turbine blade is described in Cox and Echtermeyer (2012) where the

lamination sequence used for the blade skin is provided in detail together with useful suggestions on how to model the blade in the FEM environment. Chen *et al.* (2014) also presented a FEM failure analysis of a 52.3 m composite wind turbine blade under static loading: a comparison with experimental data is carried out showing a good agreement with numerical simulations with attention to local buckling. The failure modes under static load of a 34 meters long wind turbine blade are presented in Jensen *et al.* (2006) where a comparison between FEM analysis and experimental data is provided. The spar cap stress distribution in the spanwise direction of a 38 meters long wind turbine blade is investigated in Jie *et al.* (2012). An evaluation of the resonance frequencies is also presented, with a comparison between FEM results and Block Lanczos theory. Sami *et al.* (2014) proposed a FEM to find the flapwise and edgewise modal frequency of a 5 kw glass reinforced polyester composite wind turbine blade 2.67 meters long, and compared the numerical simulations with experimental modal testing. Griffith and Carne (2010) conducted an experimental modal analysis investigation for the BSDS blade. There is a great deal of interest in the validation of FEM techniques to support wind turbine blade design analysis starting at the initial concept stage, where FEM analysis and simulations are necessary to evaluate potential configurations and structural layouts.

The rest of the paper is organized as follows: the BSDS blade CAD model is presented first, followed by a description of the FE model. A brief description of the blade test facility, the measurement setup, and the results obtained for the static and dynamic analysis of the BSDS is also included. Finally comparisons between the numerical and experimental investigation is presented along with pertinent concluding remarks.

## 2. Digital twin approach to BSDS design

The development of a BSDS digital twin model requires updating its CAD modelling, materials, and measured structural characteristics based on the results of the experimental test performed on the physical blade. The design loop implemented in this paper aims to obtain a unique digital model of the blade which can be used to robustly simulate the blade behaviour during operation. The BSDS CAD model is created from the geometric dimensions, material properties, and lamination sequence provided by the manufacturer, TPI Composites.

FEM analysis using the average data for the materials is carried out to predict the structural response of the blade. A blade corresponding to BSDS specifications was manufactured for Clarkson University. Due to blade to blade variations in manufactured blades from the reference design, the FEM model could present a structural response different from the response predicted by the design. An experimental campaign including static, modal and fatigue tests was undertaken at Clarkson to gather blade structural static/dynamic properties and responses. Since the initial numerical predictions and experimental finding were quite different, the structural model was updated to improve the

fidelity of the model to match the experiments. A digital model matching the structural response can be developed: this is useful because these models can be used to predict future behaviour of the component in different scenarios. Thanks to inspections during products lifecycle, the experimenter can evaluate the performance of the digital model. Moreover, the virtual FEM model can be updated throughout the life of the blade with performance data as to predict the effect of materials ageing or damages such as cracks and delamination of the composite, thus updating the FEM prediction capabilities. The “Digital Twin” concept applied to BSDS is presented in the following Fig. 1.

The digital twin approach is suitable for large wind turbine blades, where both blade production and installation costs can be quite significant. Changing wind turbine blades installed in remote areas is a challenging task. Large cranes are usually necessary to perform assembly/disassembly operations in large turbines. Moreover, environmental concerns can lead to the need for building temporary roads to access the operation areas, and then dismantling it to reduce the impact on the environment.

For these reasons, the real-time monitoring of turbine blades properties and future predictions, obtained from the digital twin approach, can contribute to define cost-effective and condition-based maintenance requirements. If a blade accumulates damage during operations the whole wind turbine system is at high risk, and identification of damage followed by replacement or repair of the blade is essential.

The implementation of a twin digital methodology should take into account the economic cost/benefit analysis. When dealing with small and inexpensive blades, the costs associated with performing dedicated test campaigns in expensive facilities become prohibitive, and outweigh the advantages of the digital twin approach.

In addition, inaccurate predictions due to uncertainties associated with the various computational software packages are magnified at small scales. On the other hand, this is not the case with large blades, where a positive economic impact can be obtained by implementing the digital twin concept, which can be a pillar of strategies aiming to proper condition based predicted maintenance practices.

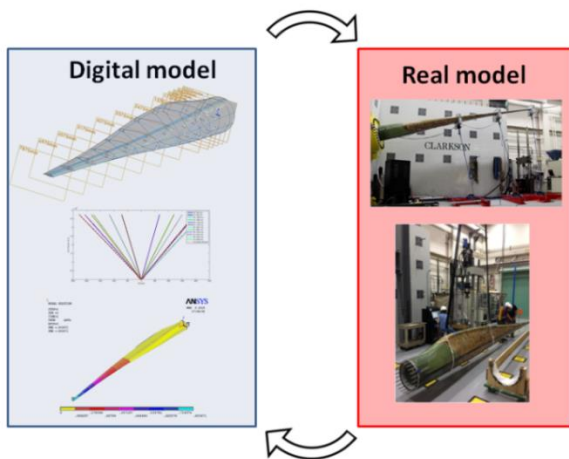


Fig. 1 “Digital twin” model of a BSDS

A different strategy could be followed where real-time monitoring is adopted. In this latter case, fibre optics or other traditional strain gauge sensors and accelerometers would be embedded in the blade during the fabrication or surface preparation with the purpose of providing continuous data in support of newly developed Industry 4.0 “data-analytics” strategies. Using data-fusion/reduction strategies significant data would be made available to the owner/operator, minimizing data overload.

### 3. BSDS blade features and CAD modelling

The optimization of a wind turbine blade account for manufacturing, structural and aerodynamic considerations. The BSDS blade design, as most blades, considered a trade-off of all these requirements.

The main innovation of the BSDS blade is the flat-back airfoil for the inboard portion of the blade. This kind of airfoil is produced by trimming the trailing edge of the blade in the inboard blade region of the blade where chord is greatest (Fig. 2, BSDS), removing the typical sharp trailing edge of the airfoil (Fig. 2, CX-100).

The advantages of flat-back airfoils include reduced weight, increased thickness, increased structural strength (especially in buckling,) and increased lift. The disadvantages include increased airfoil drag, turbulence and 3D flow, and poor aero-acoustic performance.

The noise increases with the fourth or fifth power of incident speed, while for the three-dimensional airflow and drag it is possible to use splitter plates to mitigate these effects, as proposed by Chao and Van Dam (2008). The following Table 1 shows the geometrical features of the BSDS blade investigated in this work, as provided by the manufacturer (BSDS Phase II, Blade Geometry, Rev C).

As reported in Table 1, the inboard section of the blade is based upon flat-back airfoils, while the outboard section of the blade includes high lift S830 and S831 airfoils. Due to a lack in nomenclature standardization for these flat-back airfoils, the generic name ‘FB-xxxx-yyyy’ is used to categorize these airfoils: FB refers to Flat-Back airfoil, ‘xxxx’ refers to the thickness to chord ratio and ‘yyyy’ refers to the trailing edge thickness to chord ratio.

Fig. 3 shows chord and thickness variations along the wingspan. One of the innovations concerning the BSDS blade is the presence of the constant thickness carbon fibre main spar cap, shown in Fig. 4. This spar cap is embedded in the blade shell directly over the main spar and improves the spanwise bending stiffness of the blade.

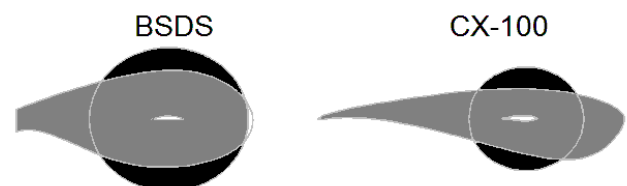


Fig. 2 BSDS and CX-100 airfoil comparison

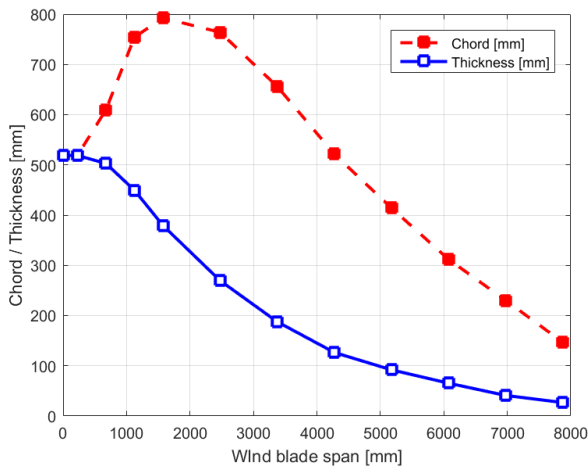


Fig. 3 Chord and Thickness along the blade span

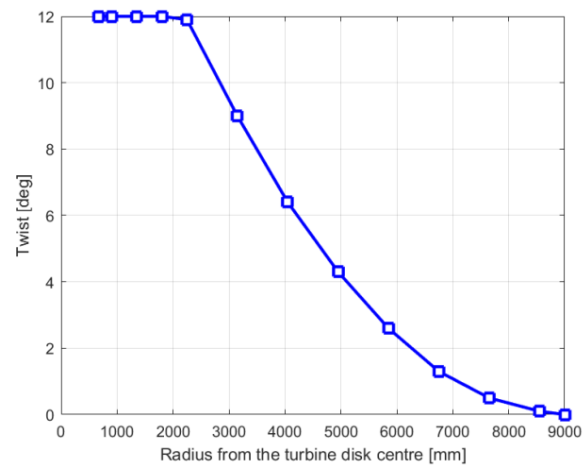


Fig. 5 Airfoil twist variation in the blade span direction

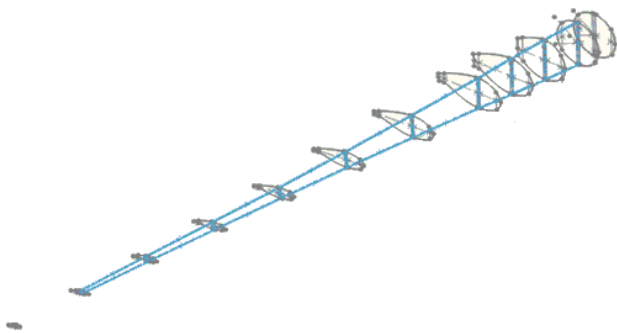


Fig. 4 BSDS Main spar

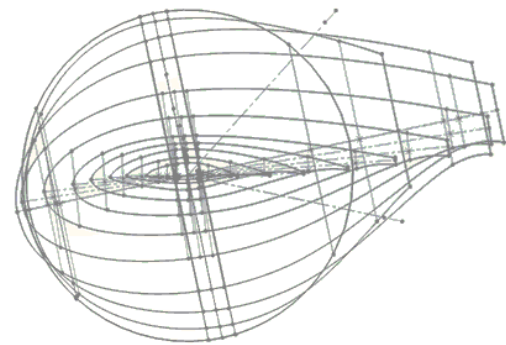


Fig. 6 Airfoils envelope

The main spar is joined to the internal surfaces of airfoil by an adhesive layer. In the BSDS blade the spar cap starts at a radius position  $R = 1\text{m}$  spanning up to  $R = 8.2\text{m}$  that corresponds in the CAD model of the blade to 10% to 85% station (see Fig. 4). The blade length is 8.325 metres, but including the hub the overall radius of the turbine is 9 meters. The origin point of the blade is at an  $r/R$  of 7.5% so all the airfoil sections have been drawn at a corresponding blade station.  $R$  is the turbine maximum radius, while  $r$  is the local radius. The external geometry of the blade was divided into three defined regions in spanwise direction: the first one is the root, a cylindrical shaped portion, the second one has a non-linear chord variation and the third one is the main body given by the flat-back airfoil and S830/31 airfoils which have linear variation chord (see Fig. 3 left). Moreover, each section was divided into 6 regions to reflect the lamination stacks over the blade's top and bottom surfaces.

The blade cross sections have been arranged along a reference line, and the twist distribution was applied to each airfoil section, as suggested by Fig. 5, where the twist distribution has been plotted. The envelope of the twisted airfoils is shown in Fig. 6.

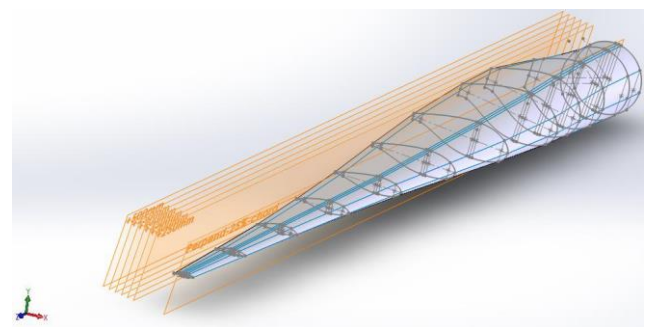


Fig. 7 Blade loft

To obtain a smooth and constant geometric silhouette along the span, a series of planes used to cut the lofted surface were used, as depicted in Fig. 7.

These cutting planes were perpendicular to the chord at blade section 25%, and located at 250 mm, 300 mm, 350mm, 400 mm, 450 mm and 500 mm from the centre-line towards the trailing edge. As already discussed, due to the changes in the laminate stacking sequence along the span, the final shell CAD model of the BSDS blade (depicted in Fig. 8) presents 7 separate surfaces, each one with a constant material stacking.

Table 1 Blade geometry and airfoils

Blade station (mm)	Chord (mm)	TE thickness (mm)	TE ratio	Thickness (mm)	Thickness Ratio	Airfoil Type
0	518.8	0	0%	518.8	100.00%	Circle
225	518.8	0	0%	518.8	100.00%	Circle
675	609.6	218.28	35.80%	502.9	82.50%	FB 8250-3580
1.125	754.38	150.85	20.00%	449.42	59.57%	FB 5957-2000
1.575	792.48	95.1	12.00%	379.14	47.84%	FB 4784-1200
2.475	764.03	45.84	6.00%	269.48	35.27%	FB 3527-0600
3.375	656.08	26.24	4.00%	187.63	28.60%	FB 2860-0400
4.275	521.46	10.8	2.07%	126.49	24.26%	FB 2426-0207
5.175	414.02	4.42	1.07%	91.92	22.20%	FB 2220-S830
6.075	311.91	0	0%	65.4	20.97%	S830
6.975	230.12	0	0%	40.94	17.79%	S830-S831
7.875	146.81	0	0%	26.82	18.27%	S831

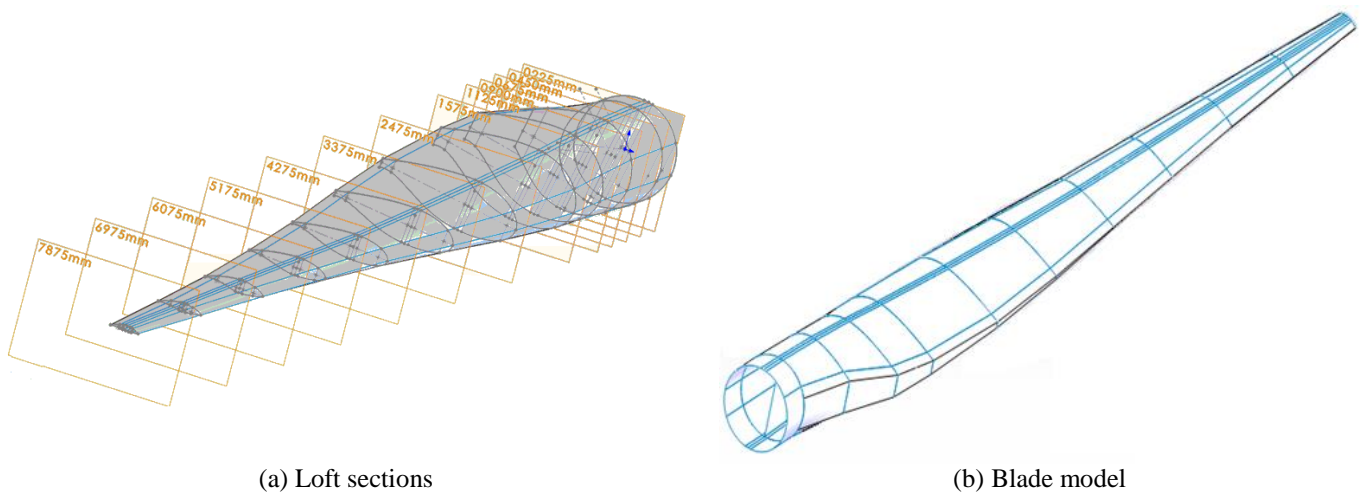


Fig. 8 Final blade CAD modelling

#### 4. FEM analyses on nominal design model

The wind turbine blade CAD model obtained is composed of a set of discrete surfaces describing the skin of the blade and spar. A shell element type was selected for the analysis as opposed to a solid element to reduce the computational time and to better model the material properties. In this case, both the skin and the spar are made by the lay-up of thin fabrics of composite or wood.

To define the properties of an element it is necessary to define material properties (which can be isotropic or orthotropic), thickness, stacking sequence and orientation about the longitudinal axis of the blade. The FEM analyses were carried out in ANSYS, using a SHELL 181 element described in the User Guide (2017) due to its good performances in handling complex stacking of materials with different properties.

Table 2 presents a list of the properties of material used to define the blade structure, as taken from the manufacturer

bill of materials. Once the material properties were defined, a laminate layup (Fig. 9) was created for the Root, Tip, and Intermediate sections, the Spar Cap, and the Spar.

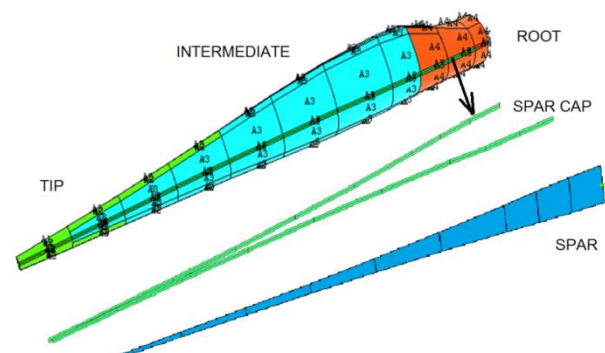


Fig. 9 Division in separate zones of the blade

Table 2 Material Properties

Material name and (ID)	$\rho$ [Kg/m <sup>3</sup> ]	$E_x$ [GPa]	$E_y$ [GPa]	$E_z$ [GPa]	$\nu_{xy}$	$\nu_{yz}$	$\nu_{xz}$	$G_{xy}$ [GPa]	$G_{yz}$ [GPa]	$G_{xz}$ [GPa]
¼ oz_mat (1)	1687	7.58	7.58	7.58	0.30	0.30	0.30	6.32	6.32	6.32
6 oz Woven glass (2)	1814	9.58	8.30	9.58	0.39	0.04	0.39	3.40	2.90	3.40
Balsa (3)	230	0.12	0.12	0.12	0.30	0.30	0.30	0.10	0.10	0.10
DBM_1208 (4)	1814	9.58	8.00	9.58	0.39	0.04	0.39	3.40	2.90	3.40
DBM_1708 (5)	1814	9.58	8.00	9.58	0.39	0.04	0.39	3.40	2.90	3.40
Gelcoat (6)	1230	3.44	3.44	3.44	0.30	0.30	0.30	2.87	2.87	2.87
Seartex (7)	1685	73.9	6.82	6.82	0.25	0.03	0.25	3.32	2.50	3.32
C520 (8)	1874	48.2	11.7	11.7	0.30	0.05	0.30	6.48	3.20	6.48
C260 (9)	1874	37.3	7.60	7.60	0.31	0.06	0.31	6.89	3.30	6.89

Table 3 Root Section

Layers	Thickness [m]	Material ID	Orientation
1	0.00051	6	0
2	0.00031	1	0
3	0.00019	5	0
4	0.00057	9	0
5	0.00037	2	45
6	0.00037	2	-45
7	0.00057	9	0
8	0.00037	2	45
9	0.00037	2	-45
10	0.00057	9	0
11	0.00037	2	45
12	0.00037	2	-45
13	0.00057	9	0
14	0.00037	2	45
15	0.00037	2	-45
16	0.00057	9	0
17	0.00037	2	45
18	0.00037	2	-45
19	0.00057	9	0
20	0.00037	2	45
21	0.00037	2	-45
22	0.00057	9	0
23	0.00037	2	45
24	0.00037	2	-45
25	0.00019	5	0
26	0.00019	5	0

Table 4 Tip Section

Layers	Thickness [m]	Material ID	Orientation
1	0.00051	6	0
2	0.00031	1	0
3	0.00057	5	0

Table 5 Intermediate Section

Layers	Thickness [m]	Material ID	Orientation
1	0.00051	6	0
2	0.00031	1	0
3	0.00019	5	45

Table 6 Intermediate Section

Layers	Thickness [m]	Material ID	Orientation
1	0.00051	6	0
2	0.00031	1	0
3	0.00087	5	0
4	0.0238	7	0

Table 7 Main Spar

Layers	Thickness [m]	Material ID	Orientation
1	0.00019	5	45
2	0.00019	5	-45
3	0.00952	3	0
4	0.00019	5	45
5	0.00019	5	-45

Tables 3-7 list the lamination stacking, material codes, orientation, and thickness in each zone of the blade.

The blade and spar geometry are meshed with a quadrangular elements with a dimension of 0.3 mm (see Fig. 10). Convergence and sensitivity analyses is carried out to ensure that the mesh sizing was correct.

A set of static and dynamic analyses are then carried out by applying a fixed constraint to the root of the blade in all displacements and rotations. This is shown in Fig. 11.

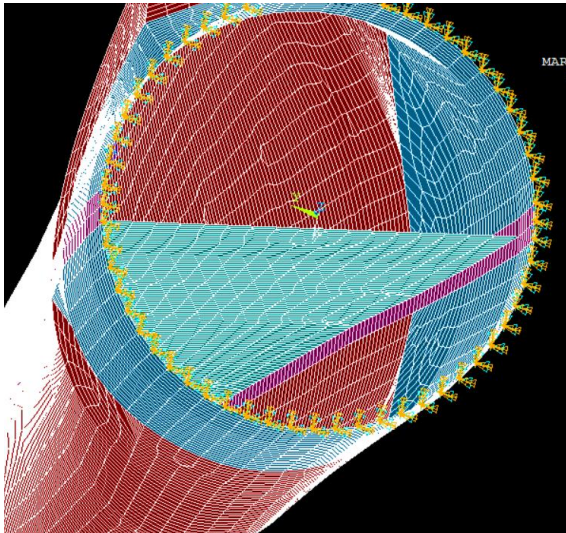


Fig. 10 Meshing of the blade in ANSYS®



Fig. 11 Constraints on the blade FEM model

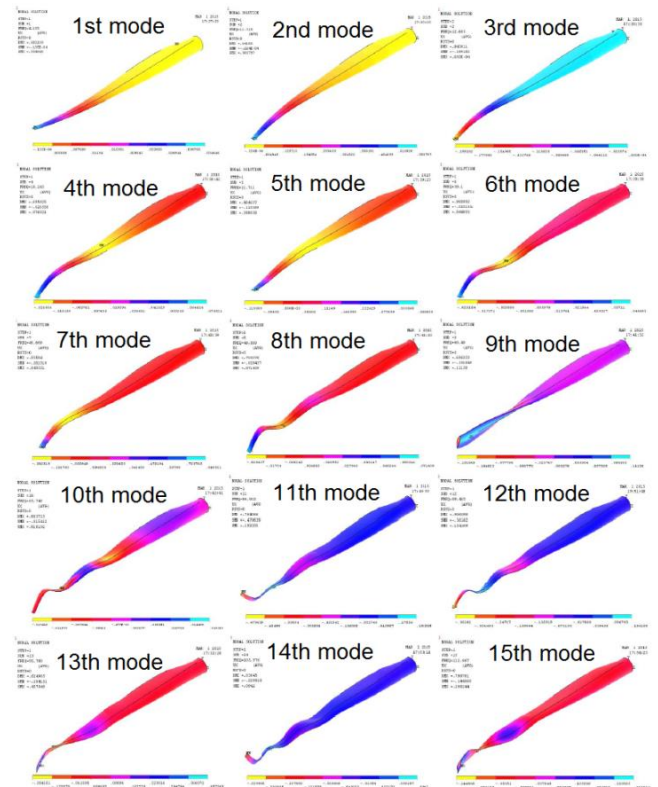


Fig. 12 First 15 BSDS natural mode shapes

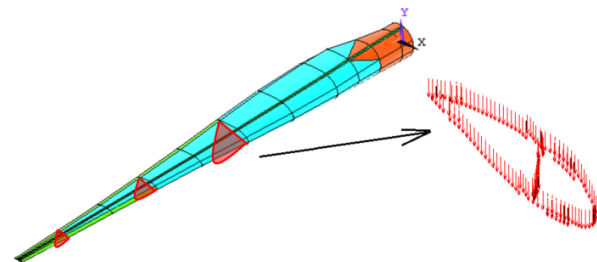


Fig. 13 Loads on saddle stations and on the single section

A first set of modal analyses was performed to determine the dynamic behaviour of the structure. Nonlinearities in material behaviour, damping, and applied loads were neglected.

The Block Lanczos method was chosen as mode extraction method: it uses an assembled stiffness and mass matrix in addition to factoring matrices that are a combination of the mass and stiffness matrices computed at various shift points. Fifteen modes between 0 and 128 Hz were computed, as Fig. 12 shows.

Static structural analysis has been carried out too. In this way, it is possible to determine displacements, stresses, strains and forces in the structure: this kind of analysis usually provides results close to the experimental ones, provided that loads in the real structure are gradually increased, thus avoiding significant inertia or damping effects.

Loads were applied in the same location where saddles have been placed in experimental analyses. The nodes along a transversal axis of the blade respect to the longitudinal axis were selected: test cases with the 25%, 50%, 75% and 100% of the load were considered.

The load was divided by the number of the nodes in the single section, as illustrated in Fig. 13.

The load cases and position of the saddles are summarized by Table 8.

Fig. 14 shows some results of the static analyses in terms of strain, while Fig. 15 illustrates the obtained displacements.

Table 8 Load cases for static analysis

Saddles location form root (m)	25% Load (kN)	50% Load (kN)	75% Load (kN)	100% Load (kN)
3	2.45	4.90	7.31	9.79
4.8	0.99	1.98	2.97	3.96
6.6	0.91	1.83	2.74	3.65

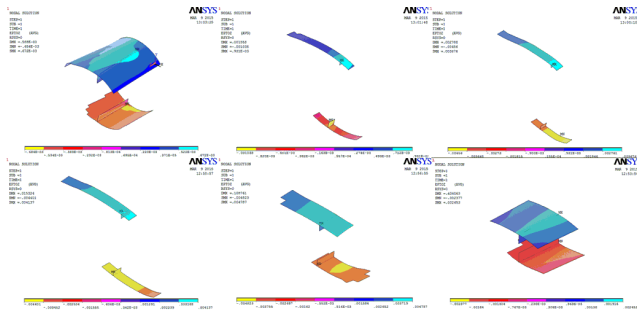


Fig. 14 Strain on the blade in a FEM test

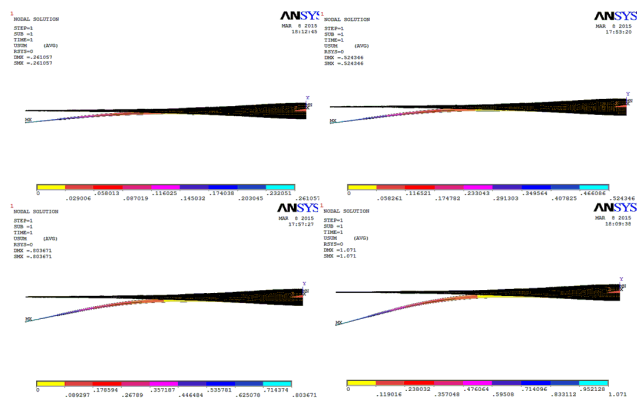


Fig. 15 Displacements on the blade in a FEM test



Fig. 16 BTF in Clarkson University

## 5. Experimental tests

### 5.1 Blade test facility (BTF)

Structural static and dynamic testing gives useful information for certification and numerical model verification. Clarkson University's Blade Test Facility (see Fig. 16) is capable of performing tests on small and mid-size wind turbine blades. The BTF is a facility consisting of three major components, the reaction frame, the hydraulic system which applies the loads, and the control/data acquisition system. The hydraulic system consists of a hydraulic power unit, hydraulic service manifold, the hydraulic actuators with servo valves, the load limiting and load abort system, and the hydraulic distribution system. The instrumentation and control system incorporates a FlexTest 60 Controller, the control system server and client PCs, the FlexDac data acquisition system, the LMS SCADAS data acquisition system and the array of sensors and wiring which interconnect the system. Three Uninterruptible Power Supplies (UPS) are used in case of emergency (one for the controller, one for the control room, and one for the data acquisition system) and four emergency are positioned in strategic locations around the test cells and control room. The supports and fixtures consist of the blade wall mounts, blade adapters, floor sheaves, blade saddles, the synthetic load chains and the strong wall itself.

The BTF consists in an 8 meter x 14 meter strong floor with two 6 meter by 5 meter reaction walls. Each is outfitted with anchorages or tie-downs that are positioned 1.2 m apart in a uniform grid. The wall is capable of sustaining a 445 kN vertical reaction and a 333 kN horizontal reaction. A pair of high strength structural steel wall mounts transfers the loads from the blade to the wall. One of them is parallel to the wall's face the other one has 15deg angle of inclination to the wall (both of them can sustain a bending moment of 1085 kN/m). Testing equipment for the strong floor includes a range of hydraulic actuators, hydraulic power supply, servo controllers, two self-equilibrating structural steel testing frames, a 979 kN Instron testing frame, a 489 kN MTS test frame, and state-of-the-art high-speed data acquisition systems. The MTS FlexTest 60 controller is an 8 channel, 2 station real-time controller with 8 valve drivers, 8 universal signal conditioners, 8 channels A/D input, 8 channels of D/A output, a dual UART interface, a 16 channel digital I/O, 2 HSM controllers, and an HPU pump control. The facility currently incorporates 6 static actuators ranging in stroke length from 0.8 m to 1.6 m and capable of loads up to 67 kN, and 2 dynamic actuators with a full range stroke of 0.6 m and a load capacity of 25 kN. The FlexDac data acquisition consists of 128 channels of 24 bit simultaneous DAQ with a synchronization timer input between it and the controller. The LMS SCADAS system includes 48 channels for both accelerometers and strain gauges measurements, 8 channels Voltage/ICP Input, internet interface for data transfer. The MTS-FlexTest controller is a real-time operating system which takes analogical signals as inputs,

outputs analogical control signals to the hydraulic components, and digital timing signals to the data acquisition equipment to maintain all data on a unified clock.

### 5.2 Modal test setup

The modal testing is based upon the measurement of the both the dynamic excitation forces and the corresponding structural responses of a structure. Two kind of modal analyses have been carried out: free-free blade and wall mounted blade. In Free-free blade modal analysis the blade was suspended by means of bungee cords to the laboratory ceiling. The test has been carried out in a frequency range 0-128 Hz, with both a modal hammer and a shaker (it has been verified that the six rigid-body motions were at frequencies lower than 0.5 Hz). The response accelerations have been measured in correspondence of 22 degrees of freedom in lateral and vertical directions, installing on the blade the same number of monoaxial accelerometers. Tests by hammer and shaker excitation have been carried out both hitting the trailing edge zone and close to the CG of the blade.

The experimental tests have been carried out by using the LMS SCADAS mobile as acquisition system, the LMS TestLAB 12A Impact Testing and MIMO FRF Testing as software for the hammer and shaker tests respectively. The LMS Polymax algorithm calculates the modal parameters from the frequency response functions. Impact tests have been carried out on the suspended blade by using a modal hammer to excite the structure at the trailing edge, close to nodes 1401 and 201. In the wall mounted blade case, an adapter plate was built to connect the blade root directly to the stand in a variety of orientations. The deformation of the adapter plate under test loads has been determined to be of negligible impact on the test results. The test was carried out by exciting the structure in either the vertical or the lateral direction at the trailing edge blade root. The response was measured in correspondence of the same 22 degrees of freedom in both lateral and vertical directions, as the previous test setup.

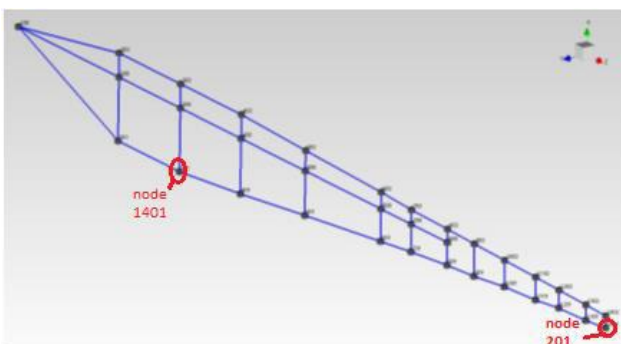


Fig. 17 Accelerometers position and excited nodes (201 and 1401)

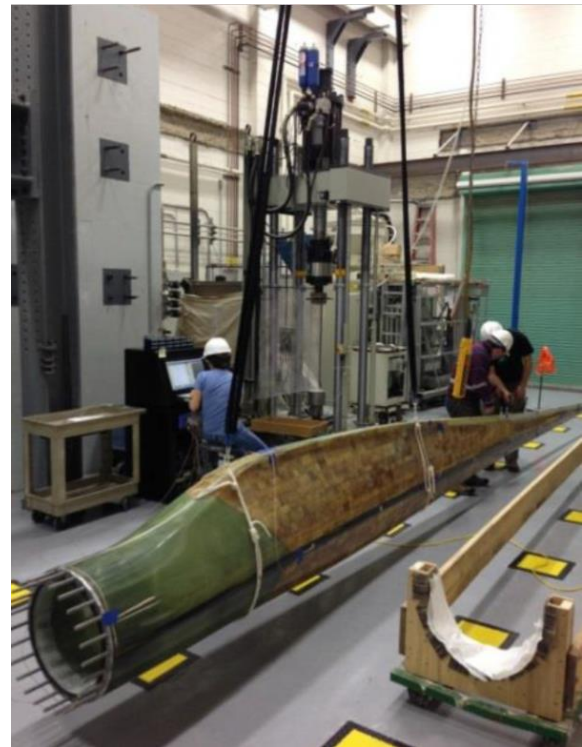


Fig. 18 Free-free blade dynamic testing in the Clarkson BTF

### 5.3 Static test

Static test is carried out to demonstrate the capability of the tested blade to sustain both its operational and extreme loading conditions. Loading in multiple directions is required as it is not possible evaluate all of the conditions with a single loading direction. A specific test plan drafted for each blade test ensure all the critical blades loads and locations tested, taking into account the loading generated by the load introduction fixturing. A simplified 2-D Euler beam element FEA analysis is conducted as part of the test design to predict deflections and calculate the required test cell geometry to ensure the blade is properly loaded and no unwanted loads generated. For an IEC 61400 blade test the blade is loaded with the design loads amplified by a factor of 1.35 to account for design load variation and material property uncertainties which generates, and resulting test loads have a further factor of 1.1 applied in certain cases to account for blade to blade variation in performance. The duration of the applied loading must be taken into account because materials may exhibit creep, a reduction of strength with duration of load. The duration of applied load should be 10 seconds at a minimum. The data acquisition hardware for the static test consist of the MTS FlexTest controller, which measures the loads and displacements from the actuators and the draw wire displacement transducers (DWDTs). The MTS FlexDac data acquisition collects the strain data for the blade and the LMS SCADAS system measures and analyses the accelerometer data for modal analysis.

Table 9 Saddles position along the wind turbine blade span

Saddle number	Saddle location (m)	Length (m)	Height (m)	Saddle mass (including load chain (kg))
1	3	0.826	0.337	65
2	4.8	0.584	0.337	45
3	6.6	0.394	0.337	35

The system sensors include a range of load cells for the hydraulic actuators, draw wire extensometers, laser displacement transducers, accelerometers, inclinometers, LVDTs, and resistive and piezoelectric strain gauges. The strain gauge type used for the blade test facility for the static test is the uniaxial gauge Vishay L2A-06-125LT-350 and three grating rosettes Vishay L2A-06-250LW-350.

The instrumentation plan includes locations on previously tested BSDS blades to enable direct comparison of measured strains. The displacements were measured using MicroEpsilon analog draw wire transducers. Three displacement transducers were used for this static test and they were placed on the ground in a location such that the wire ran parallel to the loading cable between the blade and the ground. For the static test the blade root was inclined 15 degrees above the horizontal pitch axis. The zero load condition is given by the weight of the blade, saddles, load chains and draw wire sensors without the synthetic wire rope. The load cells and the strain gauges were set in this position then were connected to the wire rope and brought to the preload condition.

The test was performed by pulling the blade downwards with a combination of gravitation deadweight acting vertically at all times and live loads cables applying force perpendicularly to the local blade neutral axis when fully loaded. The load chains were installed on the saddles and its attachment point was located directly below the centre of the LP (Low Pressure) or HP (High Pressure) spar cap respectively for each loading direction on each saddle. In this static test three saddles and turning block were used for the loading locations reported in Table 9. Fig. 19 shows one of the saddle used in the tests.

Once testing was complete the structural model of the wind turbine was updated to obtain the “Digital Twin” of the blade. The dimensional accuracy to the test article was measured to be close to the nominal values (see Table 10 for details), but the properties of material has been updated, as Table 10 shows.

Then dealing with large composite structures, a significant variability in structural properties can be observed. This is because repeatability can be hard to achieve due to material variability, hand layup and assembly, and environmental conditions.

Composite materials’ properties can change depending on material ageing and storage conditions. For example, pre-preg materials must be stored at precise low temperatures, and they have an expiration date after which the manufacturer does not guarantee their properties. Because hand laying of composite layers is the most cost

effective assembly procedure in composite parts, it is worth noting that two operations are usually performed by hand in wind turbine production.

The fabrics are hand cut, positioned and oriented/smoothed in the part mould; the component layers used for curing operations, whether it be compressing of pre-preg layups, wet layup vacuum bagging, or resin infusion methods, are prepared by hand. Even the most advanced resin infusion techniques can lead to composites embedding defects, and without an autoclave it is difficult to get void space down below 1%. It is a challenging operation to wet the composite fabric with a little as possible resin: the more resin is used, the weaker the composite is. A usual optimal ratio between resin and fabric volume is 40:60. Untrained operators can shift this ratio up to 70:30. This is especially true when no autoclave is used and therefore no pressures ranging up to 6 bars are applied to the composite to remove the excess of resin. Large autoclaves are expensive tools requiring lots of energy to keep temperatures up to 120-130 Celsius Degrees, and assuring pressure up to 7 bars, with vacuum channels to expel excess resin.

When a manual lamination is performed without autoclave (it is the usual case for large blades), it is also important to avoid trapped air in bubbles under the wet fabric, because it reduces considerably the strength of the composite. The effects of humidity, external temperature and dust embedded in the lamination, can be significant and challenging to control when resin polymerization is obtained outside an autoclave or a heated mould. For example, when wet composite temperature cures below 20 °C it is likely to cause incomplete polymerization, resulting in reduced structural properties. Taking all these issues into consideration, designing composite components is a challenging activity, requiring testing to validate structural properties. However, the FEM analyst can modify the average expected composite properties to match the experimental results. This iterative procedure is repeated until the design model predicts results sufficiently close to measured properties.

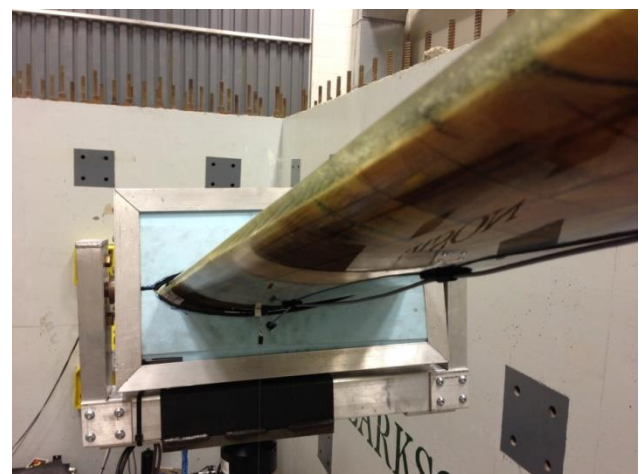


Fig. 19 Saddles configuration on the blade

Just to provide an example, the paper by Potter (2009) gives taxonomy tables listing all the possible sources of errors in composite manufacturing. The updating of material properties was guided by literature in which typical causes of material properties reduction have been widely investigated. Moreover, a knowledge of the design (e.g., stacking, lamination lay-up, materials thickness) and manufacturing process (e.g., areas where the lamination can be difficult, manual/automated processes, zones where it is difficult to obtain a good fabric to resin ratio) helps in understanding which material properties to change, and how much. The concept of Digital Twin should be extended not only to materials, but also to blade geometry. Fatigue, solar radiation, humidity, local cracking and other factors could in fact change the geometry of the blade along its operative lifespan. In this case, non-contact reverse engineering techniques based on laser or interferometry could be used to check eventual changes in the geometric model. After the blade is extracted from the mould, geometric errors can be estimated, since they are common in case of slender thin structures cured at high temperatures. In the presented case study, no significant geometric differences between nominal CAD and real model were noticed by the blade producer and since the blade was measured in the laboratory, no uncertainties on the outer mould line have been considered. The next section presents comparison data between the initial, and improved FEM models with updated materials properties.

#### 5.4 Initial model updating and comparison

In the case study presented here, material properties were updated until a good coherence between the analytical model and the experimental tests was obtained. An evolutionary, heuristic, or gradient based optimization algorithm in which material properties are changed can be used as a strategy. If the Root Mean Square error between real and FEM displacements is selected as Fitness Function, it provides a better matching between observed (real) and predicted (virtual) than a simple trial and error approach.

This section compares the experimental data of the blade as produced to the FEM analyses results of the blade as designed and to the data of the digital twin model. Table 11 shows a comparison between FEM and experimental data for saddles displacements under four levels of static loads (100% equal to 9.79 kN for Root Saddle, 3.96kN for Middle Saddle, and finally 3.65 kN for Tip Saddle) before the tuning of the digital model of the blade.

As it can be seen from Table 12 a maximum error around the 15% is found in the displacements at Root Saddle. After updating the materials properties in the FE model the improved Digital Twin model is obtained. With this new representation the maximum error in displacement is around 8% and is found at the Middle saddle values, where a slight increase in errors can be noticed.

As can be seen, implementing the Digital Twin of the blade results in a more effective prediction of the structural responses of the blade, and the virtual model can be used to more accurately simulate complex load cases. An improvement in the ability to predict blade strains has been

obtained as well. For example, Fig. 20 shows the trend of strain values along the blade prior the changes in material properties obtained by FEM and experimental analyses. Note the error in strain increases toward the blade tip.

The generation of a Digital Twin BSDS model helps to better predict the blade dynamic properties. Tables 13 and 14 present the results obtained by FEM simulation for the nominal blade (Table 13) after the changes required to obtain the Digital Twin model of the blade (Table 14) correlated to experimental data obtained from the loaded cantilever blade. The comparison between dynamic FEM and experimental data in both cases is listed below, where the symbol F stands for Flexural, L for Longitudinal, and T for Torsional.

As it can be seen from Table 14, there is a significant reduction in the errors between FEM and Experimental analyses from the nominal blade model and the “Digital Twin”, with maximum errors ranging from around the 20% to values below the 6% for the 9th mode, which is torsional.

Further analyses should be conducted by testing the blade in its mid-life, thus updating the Digital Twin by adding data relating the change of the structural properties in life due to ageing and loads. With this approach a monitoring of the structural properties of the blade could be carried out and used a reference for future blade designs, according to the philosophy of the Digital Twin concept.

Real operating blades are exposed to millions of cycles during their lifespan, which introduce damage to components and in some cases cause structural failure. Therefore, fatigue analysis became an integral part of the design process as an indicator of the service lifetime of a blade. For this study, an oscillating load of 6.01 kN, at the station located at 4.8 m from the hub has been applied to the blade up to reaching one million cycles. In this scenario, the typical behaviour of a blade is depicted by Fig. 21, where small reduction in stiffness is noticed when reaching one million of cycles. This is in agreement with the theory, where fatigue reduces the material capability of withstanding loads.

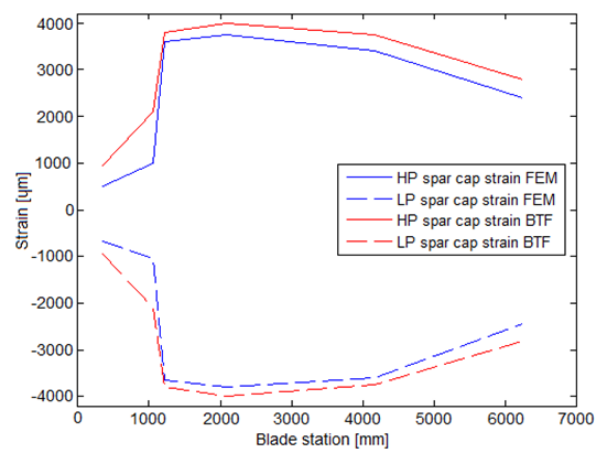


Fig. 20 Strain evaluation by FEM and Experimental Tests at lower (LP) (dashed line) and higher (HP) (solid line) spar cap along the blade span

Table 10 Update of the BSDS blade materials properties to obtain the Digital Twin

Material name and (ID)	$\rho$ [Kg/m <sup>3</sup> ]	$E_x$ [GPa]	$E_y$ [GPa]	$E_z$ [GPa]	$\nu_{xy}$	$\nu_{yz}$	$\nu_{xz}$	$G_{xy}$ [GPa]	$G_{yz}$ [GPa]	$G_{xz}$ [GPa]
¼ oz_mat (1)	1750	7.58	7.58	7.58	0.30	0.30	0.30	6.32	6.32	6.32
6 oz Woven glass (2)	1300	8.00	8.00	3.00	0.39	0.04	0.39	6.66	3.50	6.66
Balsa (3)	220	0.12	0.12	0.12	0.30	0.30	0.30	0.10	0.10	0.10
DBM_1208 (4)	1850	9.58	8.00	9.58	0.39	0.04	0.39	3.40	2.90	3.40
DBM_1708 (5)	1814	9.58	8.00	9.58	0.39	0.04	0.39	3.40	2.90	3.40
Gelcoat (6)	1230	3.30	3.30	3.30	0.30	0.30	0.30	1.27	1.27	1.27
Seartex (7)	1680	73.0	6.82	6.82	0.25	0.03	0.25	6.00	3.50	6.00
C520 (8)	1700	48.2	11.7	11.7	0.30	0.05	0.30	5.50	3.10	5.50
C260 (9)	1874	36.0	7.60	7.60	0.31	0.06	0.31	6.89	3.30	6.89

Table 11 FEM and experimental displacements of the original model

Displacements [mm]									
at Root Saddle [3 m]			at Middle Saddle [4.8 m]			at Tip Saddle [6.6 m]			
Load	FEM	Experimental	Error %	FEM	Experimental	Error %	FEM	Experimental	Error %
25%	9.67	11.48	-15.7	43.5	44.72	-2.7	130.53	134.84	-3.2
50%	19.42	22.96	-15.4	87.39	89.44	-2.3	262.17	269.67	-2.8
75%	29.76	34.72	-14.3	131.94	133.6	-1.2	401.84	405.19	-0.8
100%	39.67	46.59	-14.9	176.52	178.38	-1	535.57	540.1	-0.9

Table 12 FEM and experimental displacements of the updated model

Displacements [mm]									
at Root Saddle [3 m]			at Middle Saddle [4.8 m]			at Tip Saddle [6.6 m]			
Load	FEM	Experimental	Error %	FEM	Experimental	Error %	FEM	Experimental	Error %
25%	12.03	11.48	4.81	47.48	44.72	6.17	130.32	134.84	-3.36
50%	24.16	22.96	5.24	95.38	89.44	6.65	261.74	269.67	-2.94
75%	37.03	34.72	6.65	144.01	133.6	7.79	401.18	405.19	-0.99
100%	49.36	46.59	5.95	192.67	178.38	8.01	534.69	540.1	-1.00

Table 13 FEM and experimental predictions for nominal BSDS blade dynamic analyses

Mode	Experimental test [Hz]	FEA model [Hz]	Err [%]	Mode Description
1	3.8	4.45	+17.11	I F
2	8.48	9.63	+13.56	I L + II F
3	9.22	12.32	+33.62	II F
4	17.9	22.37	+24.97	III F
5	21.67	31.23	+44.12	II L
6	31.41	36	+14.61	IV F
7	46.06	55.43	+20.34	V F + III L
8	47.57	66.52	+39.84	III L + V F + I T
9	60.04	72.42	+20.62	I T
10	63.44	77.3	+21.85	VI F + I T

Table 14 FEM and experimental for Digital Twin blade dynamic analyses

Mode	Experimental test [Hz]	FEM model [Hz]	Err [%]	Mode Description
1	3.80	3.70	2.6	I F
2	8.48	8.22	3.1	I L + II F
3	9.22	9.60	4.1	II F
4	17.90	18.32	2.3	III F
5	21.67	22.33	3.0	II L
6	31.41	31.25	0.5	IV F
7	46.06	45.81	0.5	V F + III L
8	47.57	47.38	0.4	III L + V F + I T
9	60.04	56.53	5.8	I T
10	63.44	62.26	1.9	VI F + I T

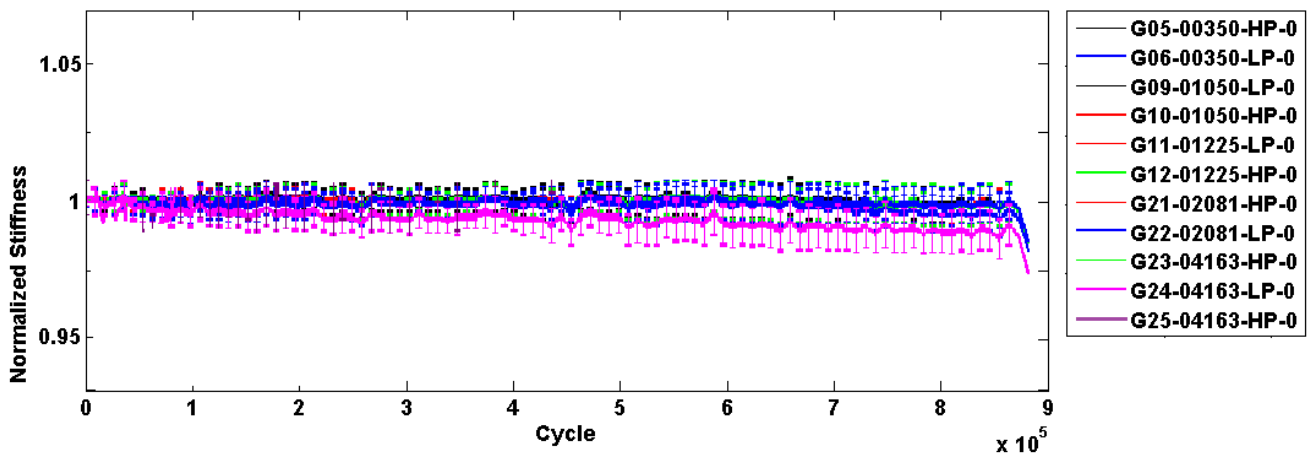


Fig. 21 Normalized blade stiffness from the experimental fatigue test

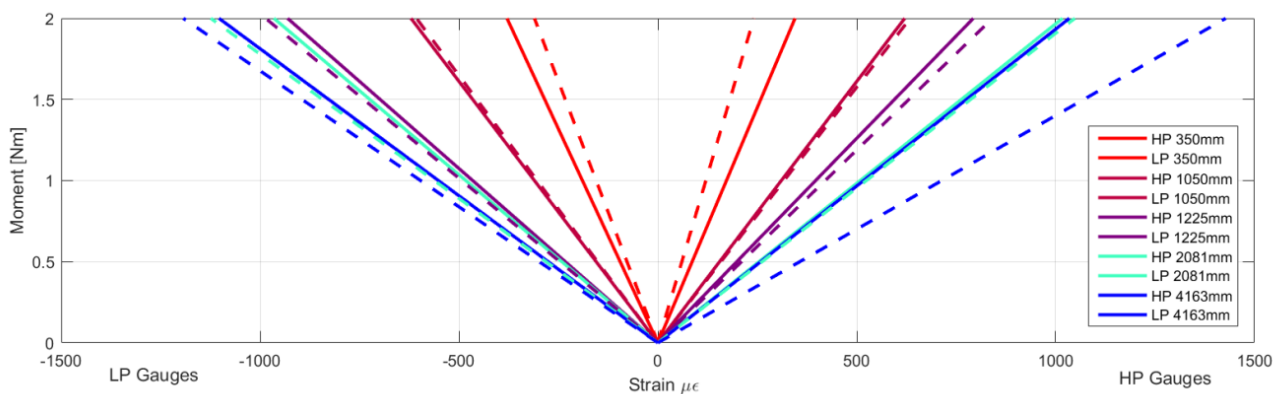


Fig. 22 Blade strain change before and after fatigue test of 1 million of cycles, measured on the spar cap, top

Fig. 22 shows the strain distribution before (solid lines) and after (dashed lines) the one million cycles load for spar caps upper surface (HP), and lower surface (LP) at selected positions from the blade hub. Experimental data showed

increased strain after the blade sustained the cyclic loading, with the exception of few locations close to the blade root. FE fatigue analysis could be performed to validate experimental outcomes, to better define loads history in operational environment (gusts, storm, pole crossing effect), and to predict future behaviour of blades. The FE model could be updated using experimental data to better

understand the fatigue behaviour of the blade, and thus improve its maintenance strategies. At periodic intervals, its dynamic performance would be updated to re-calibrate the digital model to the real one. However, a FE model for the fatigue behaviour was not implemented due to the lack of data concerning the material properties of the blade, which made it difficult to determine the S-N (strain vs number of cycles) curves needed for each of the materials to carry out the analysis.

## 5. Conclusions

This work discusses the development of a Digital Twin model for a 9 meter TPI Composites' BSDS blade. Recursive Modal and static analyses are carried out until a close agreement between virtual and real model is achieved. A high fidelity CAD model, an accurate selection of material properties, and appropriate knowledge of stacking sequence of the multi-layer composite blade structure helped to obtain satisfactory results. Good agreement between the Digital Twin and the real blade is obtained when computational simulations are compared with the experimental results attained from the free-free modal test and the wall mounted static test. When comparing the simulation of the nominal blade using design/manufacture data with the experimental results of the test article noticeable discrepancies were reported. The updated Digital Twin blade model produced a displacement error lower than 8%, and modal frequencies error under 6%. Even better agreement would be achieved using advanced algorithms tailored to optimise multiple material, structural, geometrical properties to find a minimum of a constrained nonlinear multivariate function. The Digital Twin of this blade can be further improved through a re-calibration process, obtained by taking measurements during operation or maintenance, eventually exploiting optical strain sensors embedded in the blade during lamination.

## References

- Anslys Inc. (2017), "Ansys Meshing User's Guide", available on line at: <http://148.204.81.206/Ansys/150/ANSYS%20Meshing%20Users%20Guide.pdf>, Accessed: January 2017.
- Ashrafi, M., Davoudpour, H. and Khodakarami, V. (2016), "A Bayesian network based framework to evaluate reliability in wind turbines", *Wind Struct.*, **22**(5), 543-553. <http://dx.doi.org/10.12989/was.2016.22.5.543>.
- Berry, D.S. (2008), "Blade system design study phase II: Final project report", *Sandia National Laboratories*, SAND2008-4648.
- Cerrone, A., Hochhalter, J., Heber, G. and Ingraffea, A. (2014), "On the effects of modeling as-manufactured geometry: toward digital twin", *J. Aerospace Eng.*, **2014**, Article ID 439278, 10 pages. <http://dx.doi.org/10.1155/2014/439278>.
- Chen, X., Zhao, W., Lu Zhao, X.L. and Zhong Xu, J. (2014), "Failure test and finite element simulation of a large wind turbine composite blade under static Loading", *Energies*, **7**, 2274-2297. <https://doi.org/10.3390/en7042274>.
- Chao, D.D. and Van Dam, C.P. (2008), "CFD analysis of rotating two-bladed flatback wind turbine rotor", SAND2008-1688, *Sandia National Laboratories*, Albuquerque, NM., April.
- Cox, K. and Echtermeyer, A. (2012), "Structural design and analysis of a 10MW wind turbine blade", *Energy Procedia*, **24**, 194-201. <https://doi.org/10.1016/j.egypro.2012.06.101>.
- Ghasemi, A.R., Jahanshir, A. and Tarighat, M.H. (2014), "Numerical and analytical study of aeroelastic characteristics of wind turbine composite blades", *Wind Struct.*, **18**(2), 103-116. <https://doi.org/10.12989/was.2014.18.2.103>.
- Grieves, M. and Vickers, J. (2017), "Digital twin: mitigating unpredictable, undesirable emergent behavior in complex systems", *Transdisciplinary Perspectives on Complex Systems: New Findings and Approaches*, 4 Springer International Publishing, 85-113.
- Griffith, T.D. (2010), "Experimental modal analysis of 9-meter research-sized wind turbine blades", *Proceedings of the IMAC-XXVIII* February 1-4, 2010, Jacksonville, Florida USA, Society for Experimental Mechanics Inc.
- Griffith, T.D. and Carne, T.G. (2010), "Experimental modal analysis of research-sized wind turbine blades", *Sound & Vibration*, November, [www.SandV.com](http://www.SandV.com).
- Jensen, F.M., Falzon, B.G., Ankersen, J. and Stang, H. (2006), "Structural testing and numerical simulation of a 34 m composite wind turbine blade", *Compos. Struct.*, **76**, 52-61. <https://doi.org/10.1016/j.compstruct.2006.06.008>.
- Jie, Z., Xin, C., Pan, P. and Rongrong, G. (2012), "Static and dynamic characteristics study of wind turbine blade", *Adv. Mater. Res.*, **433-440**, 438-443. <https://doi.org/10.4028/www.scientific.net/AMR.383-390.1895>.
- Luhur, M.R., Manganhar, A.L., Solangi, K.H., Jakhriani, A.Q., Mukwana, K.C. and Samo, S.R. (2016), "A review of the state-of-The-Art in aerodynamic performance of horizontal axis wind turbine", *Wind Struct.*, **22**(1), 1-16. <https://doi.org/10.12989/was.2016.22.1.001>.
- Paquette, J.A. and Veers, P.S. (2007), "Increased strength in wind turbine blades through innovative structural design", *Proceedings of the EWEC 2007 - European Wind Energy Conference & Exhibition*, Milan, Italy.
- Potter K. (2009), "Understanding the origin of defects and variability in composites manufacture", *Proceedings of the 17th international conference on composite materials*, Edinburgh, UK.
- Rezaee, M. and Aly, A.M. (2016), "Vibration control in wind turbines for performance enhancement: a comparative study", *Wind Struct.*, **22** (1), 107-131. <http://dx.doi.org/10.12989/was.2016.22.1.107>.
- Sami, S., Ahmed Zai, B. and Khan, M.A. (2014), "Dynamic analysis of a 5kw wind turbine blade with experimental validation", *J. Space Technol.*, **4**(1), 82-87.
- Seshaiah, C.V. and Sukkiramathi, K. (2016), "A Mathematical model to estimate the wind power using three parameter Weibull distribution", *Wind Struct.*, **22**(4), 393-408. <https://doi.org/10.12989/was.2016.22.4.393>.
- Tartibu, L.K., Kilfoil, M. and Van Der Merwe, A.J. (2012), "Modal testing of a simplified wind turbine blade", *IJAET Int. J. Adv. Eng. Technol.*, 649-660.
- Valyou, D.N, Arsenault, T.J., Janoyan, K., Marzocca, P., Post, N., Grappasonni, C., Arras, M., Coppotelli, G. Cardenas, D., Elizalde, H. and Probst, O. (2015), "Development and commissioning of a small / mid-size wind turbine test facility", *Proceedings of the 33rd Wind Energy Symposium, AIAA SciTech Forum*, (AIAA 2015-1000).